RESEARCH ARTICLE

Identification of the Binding Interaction of Anti-tuberculous Drugs with Human Serum Albumin: A Computational Molecular Docking, Fluorescence and Absorption Spectroscopy Study

Sarfaraaz Vallie*, Sivapregasen Naidoo

Stellenbosch University, Division of Clinical Pharmacology, Western Cape, South Africa

Received: 21st Dec, 2019; Revised: 21st Jan, 2020; Accepted: 18th Feb, 2020; Available Online: 25th Mar, 2020

ABSTRACT

The accuracy in Anti-tuberculous drug assaying was supported by computational modeling using a 2 and 3-dimensional thermodynamic binding affinity prediction of each drug during multiple drug co-administration regimens. The United States Food and Drug Administration has highlighted the need for extensive research to improve the recovery during analytical drug method development, where the recovery affects the slope of the calibration curve. Here we focused on the drug-protein binding variation that affects the extrapolation of the patient sample drug concentration from the slope of the calibration curve. The binding constants calculated at a physiological temperature from the fluorescence spectroscopy data were as follows: Rifampicin 5.379 X 10^2 M^{-1} (moderate affinity), Isoniazid 9.285 M^{-1} (low affinity), 25-Desacetyl Rifampicin 3.156 M^{-1} (low affinity), Ethambutol 3.443 M^{-1} (low affinity) and Pyrazinamide 3.076 X 10^2 M^{-1} (moderate affinity). These drugs Gibbs free energy were below zero, indicating spontaneous binding reactions. Rifampicin a non-polar weak acid with a higher affinity indicating the most stable complex formation with albumin as opposed to soluble Isoniazid due to it being polar and an ionized form to be easily excreted in the urine resulting in low levels of detection. This will affect the bioavailability and accuracy of the assay levels for patients experiencing hyper and hypoalbuminemia with related competition and induction processes of the enzymes. These complications are apparent where larger numbers of patients are involved in clinical trials, bioequivalence and bioavailability studies with varying protein levels that may be more crucial for drugs with a narrow therapeutic index.

Keywords: Absorbance spectroscopy, Anti-TB drugs, Computational modeling, Fluorescence spectroscopy, Human serum albumin, Thermodynamic binding interactions.

International Journal of Pharmaceutical Quality Assurance (2020); DOI: 10.25258/ijpqa.11.1.1

How to cite this article: Vallie S, Naidoo S. Identification of the Binding Interaction of Anti-tuberculous drugs with Human Serum Albumin: A Computational Molecular Docking, Fluorescence and Absorption Spectroscopy Study. International Journal of Pharmaceutical Quality Assurance. 2020;11(1):1-14

Source of support: Nil

Conflict of interest: None

INTRODUCTION

Patient blood protein levels play a critical role in bioanalytical calibration curve extrapolation accuracy. The proteins levels are also essential biomarkers where albumin is classified as marked hypoalbuminemia (<2.5 g/dL), mild hypoalbuminemia (2.5–3.5 g/dL), normal albumin (3.5-4.5 g/dL), and hyperalbuminemia (>4.5 g/dL).[1] In this study, we aimed to optimize the drug assay accuracy in multiple drug regimens in patients with varying protein content due to disease and illness. By understanding and identifying the binding interactions of first-line anti-tuberculosis (TB) drugs to human serum or plasma albumin, we will be able to gain insight and further understand the protein evaluation significance in calibration curve extrapolation inaccuracies. TB is highly contagious and spreads through the airborne particles, couching, fluids, and exposure to various other contaminations opportunities. TB is caused by a bacterium known as Mycobacterium tuberculosis, which is rod-shaped in structure.[2] The first line anti-TB drugs and the rifampicin (RIF) metabolite 25-desacetyl rifampicin's (D-RIF) binding interactions with human serum albumin via computational modeling and with plasma via Fluorescence spectroscopy and Ultraviolet spectroscopy were investigated. It is the most common cause of death by the infectious disease worldwide. The most common infected site for TB is known as the pulmonary tract.[3] Myco TB is a disease that can be cured by using a number of specific antibiotics prescribed. The treatment consists of multiple numbers of drugs that have to be taking over a period of 6 months and can even be extended to 12 months. The US Food and Drug Administration (FDA) approved ten drugs at this current stage for the treatment of Tuberculosis. Four of the ten drugs are used in first-line

**Author for Correspondence: sarfaraaz.vallie@gmail.com*

anti-TB treatment. The four drugs are namely: isoniazid (INH), rifampicin (RIF), pyrazinamide (PYR), and ethambutol (ETH)) (RIF-4). These four drugs form the foundation of the initial stages of TB treatment.[4,5]

The HSA is a major protein component of plasma responsible for the transportation and storage and disposition of compounds or ligands in the blood.[6,7] HSA has a heart conformation 3D geometrical shape consisting of 585 amino acid residues in a single polypeptide chain.[8,9] HSA has three domains connected via 17 disulfide bridges, which can be divided into subunits (I, II, and III) and represent a similar alpha-helical shape.[10] Each of the three HSA domains can be further separated into sub-domains A, and B.[11] Two principle ligand binding sites within the HSA protein can be found in subdomains IIA and IIIA known as Sudlow's site I and II respectively. Furthermore, a binding site was identified in subdomain IB.[12] The basic residues (Lys195, Lys199, Arg218, Arg222) surround the opening of site 1 however, the bottom of the site is hydrophobic. An important residue tryptophan 214 often for structural analysis is also present at site 1. Site II is much smaller in size comparatively and accommodates the binding of hydrophobic drugs due to the predominate hydrophobic residues present.[13-16] A study conducted by Ping Li, according to the free drug theory it states that in an in-vivo system, the drug interchanges from protein-bound to unbound states through reversible rapid equilibrium processes. When the drug is distributed to the circulatory blood-stream, only the free unbound drug can permeate through the tissue to the active or target site, which produces its effect and, after some time reaches its half-life. In studies conducted through in-vitro plasma-protein binding studies, the data is often used to understand and replicate the in-vivo phenomena. This practice provides information in clinical and medicinal sciences, which aids in optimizing patient selection in trials. The problem faced with this practice is that the binding kinetics which occur in living systems is neglected. These kinetic binding effects have great influences on the pharmacokinetic and pharmacodynamics. Thus the insight into the interaction between First-line anti-TB drugs and HSA becomes important.[17]

According to a review article in fluorescence studies a common methodology is used to conduct binding studies: A suggestion made that the chosen ligands is to bind to a fluorescent protein, the addition of the ligand to the protein quenches the fluorophore present in the protein, the use of the stern-vomer equation generates a large bimolecular rate constant which cancels out collisional quenching and indicates that ligand binding occurs, the binding constants are then quantified. However, it is important that the following is acknowledged when conducting binding studies: the inner-filter effect, collisional quenching, and binding related changes.[40] In this study, we focused on the anti-TB drug interaction with other components as well in the plasma, including HSA and fatty acids, for the effects of linearity in calibration curves. The methodologies mentioned earlier do not fall within the scope of this research as we use a single methodology, and we did not compare different methodologies.

The aim of this study was to identify and understand the binding interaction mechanism of the first-line anti-TB drug INH, RIF, PYR and ETH and 25-desacetyl rifampicin (D-RIF) a major metabolite of RIF with HSA using molecular docking, spectroscopic and thermodynamic approaches. We wish to confirm the binding affinity of different drugs with different pKa values to establish a more accurate protein evaluation in calibration curves. This affects the recovery and accuracy of calibration curves. Narrow therapeutic drugs, bioequivalence and bioavailability studies are most affected by the less than 100% recovery. When administering first-line anti-TB drugs systemically, it has been indicated in literature that a specific part of the drug interacts with the protein present in plasma.[18] These types of interactions take place via hydrogen bonding, weak Van de Waal interactions, electrostatic interaction, and covalent bonding.[19] These types of interactions could cause changes to the drug or even increase the half-life of the drug before reaching the site of action.[20-24] This could result in a better understanding to advances in anti TB resistance and first–line anti-TB drugs. We aimed to show the difference between HSA and plasma content, where plasma does contain other components that affect fluorescence quenching.

EXPERIMENTAL

Materials

RIF, INH, ETH, PYR, and D-RIF reference materials were obtained from international supplier Sigma Alderich. The plasma used was obtained from the Tygerberg Hospital in Bellville, Cape Town, South Africa, from blood donor patients. All samples were prepared in a phosphate buffer system with a (pH 7.4 with final concentration of 10 mM PO_4^{3-}, 137 mM NaCl, and 2.7 mM KCl). All reagents used were of analytical grade and Milli pour distilled water was used throughout the experiment.

Instruments

Molecular operating environment (MOE) and Pymol computer software were used to conduct computational prediction studies. The Fluorescence and UV spectroscopy studies were conducted using an Omega Fluorostar spectroscopic instrument from BMG LABTECH. The Fluorescence emission spectra ranged from 300-700 nm with an excitation wavelength fixed at 278/9 nm. The emission spectra were recorded of human blood Plasma with and without each drug. The UV absorbance spectra ranged from 220-650 nm. The absorbance spectra were recorded for human blood plasma with and without drug present. The sample runs were conducted using a 96 well plate. The pH measurements were conducted using a calibrated digital pH meter. All spectra were measured at a temperature range of 298.15 K, 310.15 K, 313.15 K and 318.15 K.

Molecular Docking Preparation

Computational modeling in pharmacology is a technique that has been recently developed. It is a technique that is based on theoretical pharmacological aspects and modeling of many molecules.[25] It is aimed towards rationalizing the relationship between the drug activities when observed experimentally and it structural features derived from computational chemistry

and molecular mechanics. The main use of this technique is to provide valuable, efficient, accurate, and cost-effective alternative methods for drug study and development.[25] Computational pharmacology is used to determine the possible binding action of molecules within the protein pockets of a specific protein. The protein macromolecule is usually obtained from a protein data bank.[26] This protein data bank has already modeled the protein structure to the atomic scale.[25] The ligands that bind to the protein pockets are required to be modeled by the use of a computation pharmacology operating system. The modeled ligands are then docked to the protein pocket according to the most probable binding interaction of the ligand and the protein.[25] The operating system is also responsible for the prediction of the possible interaction between the ligand and the protein pocket site. This interaction can be illustrated in 3D and 2D.[26] The 2-D interaction generated indicates specifically how the ligand binds to the pocket of the protein as well as the interaction or binding of the ligand to the amino acid.[27,28] The 3D surface topography can be illustrated in different modeling imagery such as ribbons, cartoon, or surface topology imagery, and many more.[23,]28 When docking the ligand to protein the process undergoes a search of different positions and conformations within the protein pockets available, which generates scores to calculate the binding affinity of the ligand to a specific side chain.[25,27,29] The search program is an algorithm that proposes the degree of freedom of the protein-ligand interaction complex. Hence it can be used to rank binding interactions of different molecules and the thermodynamic interactions between the ligand and the protein predicted from these scores.[29, 30]

In this study, the computer software for prediction of the possible binding sites of the drug to HSA used was MOE. Each drug was constructed and modeled according to its molecular weight and computational codes were build, which corresponded to each drug in question. Molecular docking feature of MOE is used to predict how the Van de Waals forces, hydrogen bonding and electrostatic bonding interaction of the ligands to the protein pocket binding site as the ligands spacial position and orientation can be changed in the binding pocket of the host.[28, 31] Thereafter a full molecular minimization mechanics can be done using the universal force field to indicate the possible binding interaction energy of the specific drug to the HSA binding site. The aim of docking the drug to HSA is to conform the drug to the HSA binding site to get the lowest possible enthalpy value.[32] The HSA protein used was obtained from the protein data bank. The HSA protein used was HSA PDB-1E7I as indicated in Figure 1. The constructed molecular protein modeling was then extracted using the 3D software viewer Pymol. In this experiment, enthalpy values were obtained for each drug. The entropies, as well as the Gibbs free energies, were calculated via the use of the possible enthalpy values obtained.[32] The temperature used was predicted to be body temperature of 37ºC or 310.15 K.[33] The predictions generated from the MOE software were compared to the experimental thermodynamic properties and interactions generated from the fluorescence spectroscopy and ultraviolet (UV) spectroscopy experimental data obtained of the drugs of interest when interacting with blood plasma proteins.[34]

The MOE software requires smiles, which is an algorithm that represents each drug: RIF, INH, PYR, ETH, and D-RIF. The compounds are then docked to the HSA 1e7i protein from the plasma, which was obtained from the protein data bank. The computer software for prediction of the possible binding affinity and mode of the drug to HSA used was MOE. The molecular docking studies were performed by using MOE software, is an interactive molecular graphics program to understand the drug-protein interaction. The structure of the complex was sketched by CHEMSKETCH (http://www.acdlabs.com) and converts it into pdb file format from mol format by OPENBABEL (http://www.vcclab.org/lab/babel/). The crystal structure of the Human Serum Albumin (PDB ID: 1E7i) was downloaded from the protein data bank (http://www.rcsb.org./pdb). All calculations were performed using a Microsoft PC operating system. Visualization of the docked pose was performed by using PyMol molecular graphic program (http://www.pymol.sourceforge.net/). In this computational modeling experiment, ΔH° values were obtained for each drug. The entropies, as well as the Gibbs free energies, were calculated via the use of the *predicted* ΔH° values obtained. The temperature used was predicted to be body temperature of 37ºC or 310.15 K.

Sample Preparation for Fluorescence and UV Spectroscopy Analysis

The following drugs: RIF, INH, PYR, ETH, D-RIF, and RIF-4 were made up in Phosphate buffer to a concentration of 100 µg/ml. Further dilutions were made to each stock solution ranging from 1-30 µg/mL in increments of 5. Each dilution contained 0.5 ml of plasma. Each drug was soluble in the phosphate buffer (pH 7.4 with a final concentration of 10 mM PO_4^{3-}, 137 mM NaCl, and 2.7 mM KCl)

RESULTS AND DISCUSSION

Computational Modeling and Binding Interactions of Drugs to HSA Protein and Fluorescence Spectroscopy of Drugs Interacting with the Plasma

The following the computational and binding interactions obtained from Table 1 were a statistical computational prediction of how RIF, D-RIF, INH, PYR and ETH would bind to the HSA protein. This type of statistical data is defined as computational molecular predictive ligand-protein interaction. This computational software aims to provide the best and most probable interactions that the drug could be exposed to when being in the presence of the HSA and plasma proteins. From the data predicted data obtained, it was observed that all the drugs could undergo spontaneous reactions with HSA as a result of the negative Gibbs free energy values obtained. This was acquired using the predicted enthalpy values obtained for each drug and by calculation of the entropy and the Gibbs free energy, as indicated in table 1 by the use of equations 1 and 2.

The fluorescence spectroscopy data was obtained experimentally for the drugs INH, RIF, D-RIF, PYR, ETH and RIF-4 using human blood plasma samples to obtain the experimental Enthalpy, Entropy and Gibbs free energy values based on the actual Drug interacting with human Plasma protein samples which was then compared to the to the predicted interaction of the drugs with HSA protein which is a protein present in plasma.

$$\Delta S° = -\frac{\Delta H°}{T} \quad \text{...Equation 1}$$

$$\Delta G° = \Delta H° - T\Delta S° \quad \text{...Equation 2}$$

According to literature, the enthalpy and entropy thermodynamic parameter can be used to explain interactions between molecules and protein.[34] A positive enthalpy is an indication of hydrophobic interaction.[34] Whereas a negative enthalpy coupled with positive entropy is an indication of electrostatic interaction between ionic species.[34] Whereas negative enthalpy and entropy indicate evidence of weak Van de Waal interactions and hydrogen bonding taking place.[34] However, molecules can interact via hydrogen bonding and electrostatic interactions.[35] From the predicted data in table 1, The following Gibbs free energy was obtained for INH, RIF, D-RIF, PYR, and ETH. The predicted Gibbs free energy negative values obtained as illustrated in table 1 indicated that all the drugs undergo spontaneous interaction with HSA.[34] RIF indicated the lowest energy required, and PYR indicated the highest energy required for interaction with HSA to take place. The predicted enthalpy and entropy produced positive and negative values, respectively. This was an indication that the drug interaction of all drugs assessed possibly interacted electrostatically with the HSA protein. RIF indicated the strongest electrostatic interaction from the predicted results, and PYR indicates the weakest electrostatic interaction with HSA.

The 3-D Pymol best interaction of INH bound to the HSA protein is illustrated in Figure 2a). In Figure 2b) Tyrosine-161 amino acid residues and the nature of the interaction between INH and HSA. In Figure 2c), the hydrogen present on the side chain Hydrazine functional group of the INH drug interacts with acidic tyrosine amino acid 161 group present in HSA protein, this indicates possible hydrogen bonding and electrostatic interaction is taking place. This interaction occurs because the tyrosine amino acid hydroxyl group is polar due to the pH 7.4 environment, which causes deprotonation of the hydroxyl group causing the hydroxyl group to be negatively charged. The INH hydrazine group in the pH environment is ionized, which allows for the hydrogen interaction to occur between the INH hydrazine group and the Tyrosine amino acid hydroxyl group. The experimental data obtained from the Fluorescence spectroscopy spectrum analysis of INH with plasma indicated that as the concentration of drugs increased in the plasma sample, the fluorescence spectroscopy spectrum decreased as indicated in Figure 2 d). This is an indication that INH quenches the plasma proteins present in the sample.

The binding interaction of RIF to the HSA binding pocket is indicated by the Pymol image in Figure 3 a). In Figure 3 b) Asparic-451, Arginine-218, Arginine-257 and Lysine-199 and the nature of the interaction between RIF and HSA are indicated. In Figure 3 c). The MOE 2D interaction illustrates possible hydrogen bonding of an OH group present on the RIF drug with the polar exposed Aspartic amino acid 451 residues of HSA. Aspartic acid is a few of the only standard amino acids which contained a carboxylic acid group in the side chain of the amino acid. In the pH environment, the functional groups of Aspartic acid are usually negatively charged due to the approximate pKa value of 4. The pKa for the hydroxyl group of RIF is 1.7.[36]. Therefore this will allow for hydrogen bonding and electrostatic interaction occurring between the two polar molecules RIF and the amino acid Aspartic acid. The experimental data obtained from the Fluorescence spectroscopy spectrum analysis of RIF with plasma indicated that as the concentration of drugs increased in the plasma sample, the fluorescence spectroscopy spectrum decreased

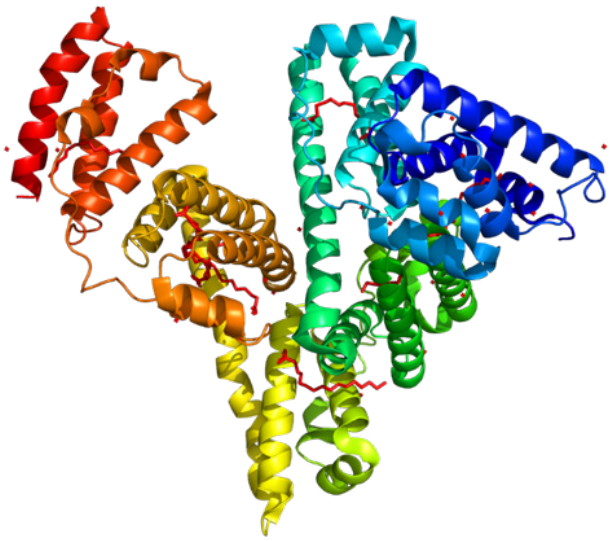

Figure 1: HSA 1e7i protein modeled structure

Table 1: Predicted Enthalpy, calculated entropy, and calculated Gibbs free energy values based on the most probable interaction of the drugs: INH, RIF, D-RIF, PYR, and ETH to bind to HSA protein pocket site.

Drug	*Predicted Enthalpy (ΔH°) (kJ/mol)*	*Calculated Entropy (ΔS°) (KJ/K)*	*Calculated Gibbs free energy (ΔG°) (kJ/mol) rounded off to 4 decimals*
INH	-25.994383	0.08381229405	-51.9888
RIF	-52.020626	0.16772731260	-104.0413
D-RIF	-38.404728	0.12382630340	-76.8095
PYR	-16.525791	0.05328322102	-33.0516
ETH	-40.259628	0.12980599060	-80.5190

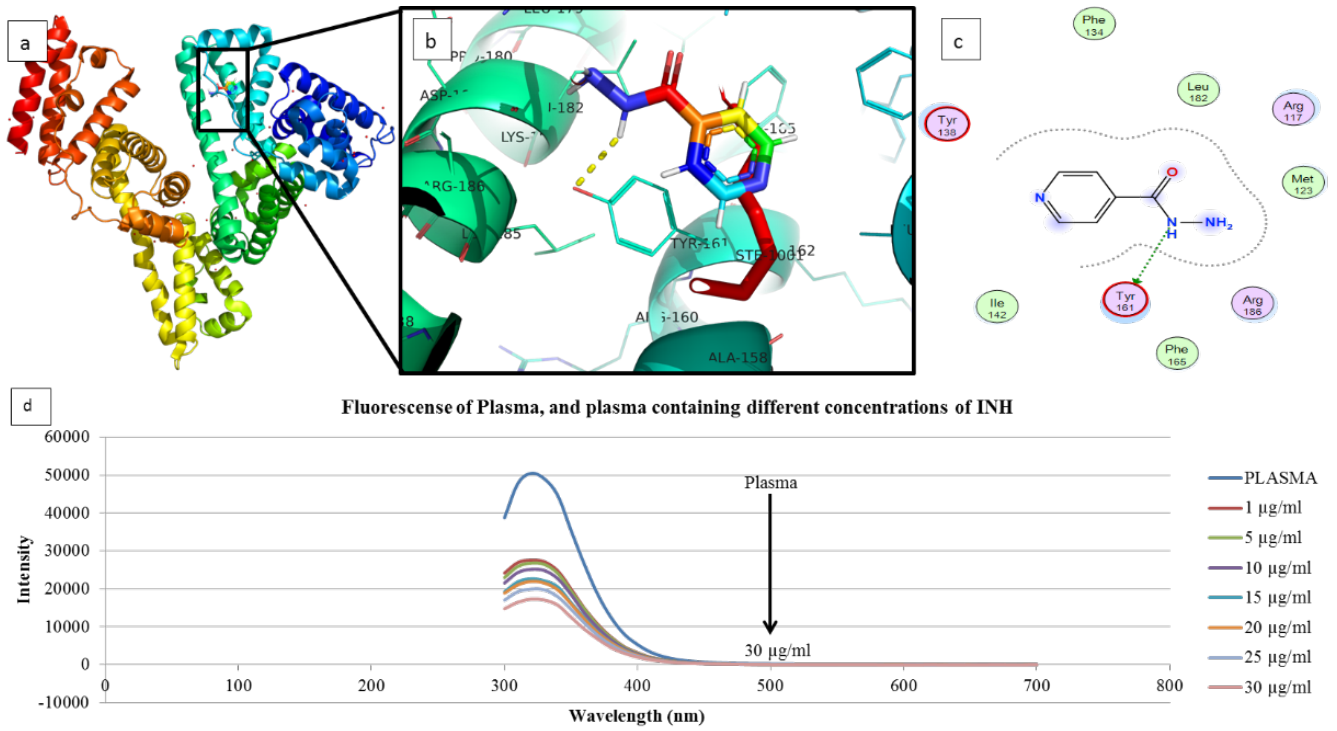

Figure 2: INH interactions a) Predicted Pymol 3D interaction of INH with HSA protein binding pocket. b) Amino acid residues and the nature of the interaction between INH and HSA. c) MOE interaction of INH with HSA protein pocket d) Experimental fluorescence spectroscopy interaction of INH in plasma at a concentration range of 1µg/ml-30µg/ml in increments of 5µg/mL compared to pure plasma standard

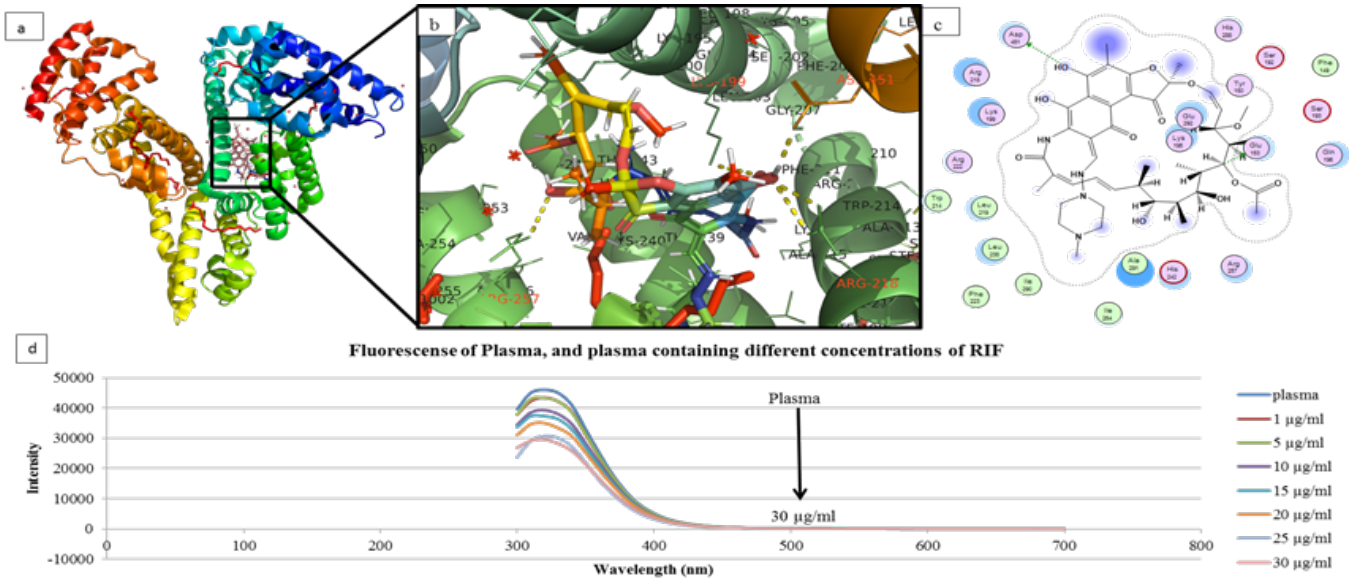

Figure 3: RIF interactions a) Predicted Pymol 3D interaction of RIF with HSA protein binding pocket. b) Amino acid residues and the nature of the interaction between RIF and HSA. c) MOE interaction of RIF with HSA protein pocket d) Experimental fluorescence spectroscopy interaction of RIF in plasma at a concentration range of 1µg/ml-30 µg/ml in increments of 5µg/mL compared to pure plasma standard

as indicated in Figure 3d). This is an indication that as the concentration of RIF increases, the quenching of the plasma proteins present in the sample increases, and the fluorescence spectroscopy emission of the plasma decreases.

For the metabolite of RIF D-RIF, the Pymol 3-D interaction indicates the most probable site of interaction of D-RIF and the HSA binding pocket, as indicated in Figure 4 a). In Figure 4 b) Amino acid residues phenylalanine-206, arginine-209, and the nature of the interaction between RIF and HSA. In Figure 4c) The MOE 2D D-RIF, which represents possible hydrogen bonding and electrostatic interaction between the NH group of D-RIF as a backbone donor to the greasy exposed HSA phenylalanine 206 amino acid occurs. Another possible interaction occurs where the hydrogen group with an exposed amino acid Arginine 209 could be a result of weak electrostatic interaction. The experimental data obtained from the

Fluorescence spectroscopy spectrum analysis of D-RIF with plasma indicated that as the concentration of drugs increased in the plasma sample, the fluorescence spectroscopy spectrum decreased as indicated in Figure 4 d). This is an indication that as the concentration of D-RIF increases, the quenching of the plasma proteins present in the sample increases, and the fluorescence spectroscopy emission of the plasma decreases.

PYR illustrates binding interaction with HSA binding site in the pymol 3d image in Figure 5 a). In Figure 5 b) Amino acid residues Arginine-117, Leucine-182, Tyrosine-161, and the

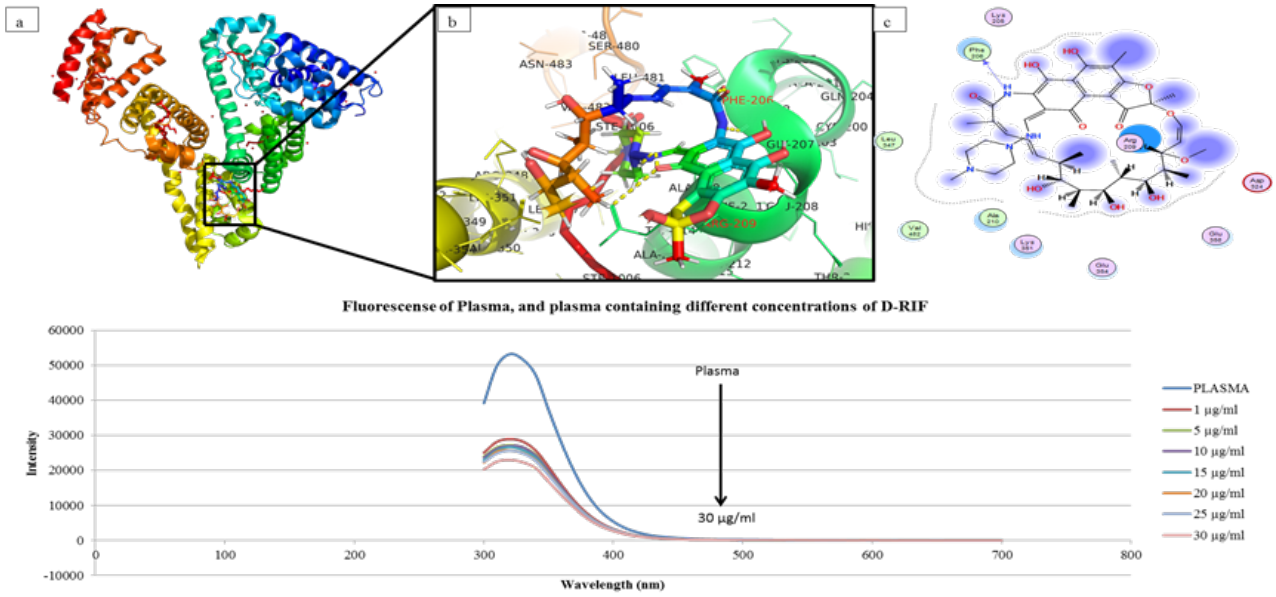

Figure 4: D-RIF interactions a) Predicted Pymol 3D interaction of D-RIF with HSA protein binding pocket. b) Amino acid residues and the nature of the interaction between D-RIF and HSA. c) 2D MOE interaction of D-RIF with HSA protein pocket d) Experimental fluorescence spectroscopy interaction of D-RIF in plasma at a concentration range of 1µg/mL-30 µg/ml in increments of 5µg/ml compared to pure plasma standard

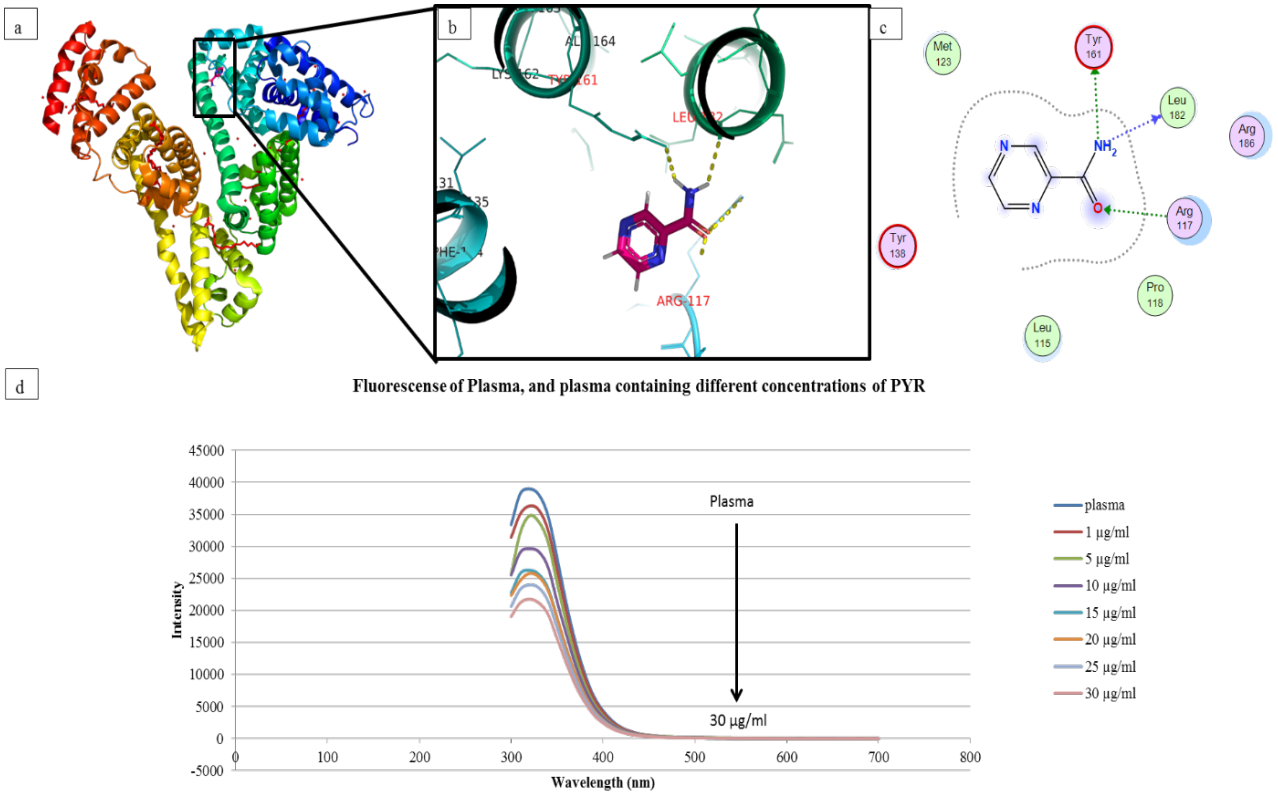

Figure 5: PYR interactions a) Predicted Pymol 3D interaction of PYR with HSA protein binding pocket. b) Amino acid residues and the nature of the interaction between PYR and HSA. c) MOE interaction of PYR with HSA protein pocket d) Experimental fluorescence spectroscopy interaction of PYR in plasma at a concentration range of 1µg/ml-30 µg/ml in increments of 5µg/ml compared to pure plasma standard

nature of the interaction between PYR and HSA are illustrated. The 2D MOE interaction in Figure 5 c) indicates possible interaction by hydrogen bonding and electrostatic interaction, between the NH_2 group present in the PYR molecule as a side chain donor to the acid tyrosine 161 amino acid, between the NH_2 as a backbone donor to the greasy Leucine 182 amino acid residue and the oxygen group present in the PYR molecule as a side chain acceptor from the Arginine 117 side-chain donor amino acid. The experimental data obtained from the Fluorescence spectroscopy spectrum analysis of PYR with plasma indicated that as the concentration of drugs increased in the plasma sample, the fluorescence spectroscopy spectrum decreased as indicated in Figure 5 d). This is an indication that as the concentration of PYR increases, the quenching of the plasma proteins present in the sample increases, and the fluorescence spectroscopy emission of the plasma decreases.

The 3D Pymol predicted interaction with HSA protein is illustrated in Figure 6 a). In Figure 6 b) Amino acid residue Tyrosine-411 and the nature of the interaction between ETH and HSA. In Figure 6 c), the 2D MOE interaction indicates that possible hydrogen bonding and electrostatic interaction occurs via the NH and OH functional groups of ETH with the acidic tyrosine 411 amino acid as side-chain donors. The experimental data obtained from the Fluorescence spectroscopy spectrum analysis of ETH with plasma indicated that as the concentration of drugs increased in the plasma sample, the fluorescence spectroscopy spectrum decreased as indicated in Figure 6 d). This is an indication that as the concentration of ETH increases, the quenching of the plasma proteins present in the sample increases and the fluorescence spectroscopy emission of the plasma decreases. As a result, it can be identified that all 4 TB drugs and the metabolite of RIF induce the same effect of quenching plasma; however, the magnitude of each quencher drug differs.

Another parameter was assessed by conducting fluorescence spectroscopy on the 4 TB drug RIF-4. In Figure 7, the same trend was observed that as the concentration of drugs increased within a plasma, the fluorescence spectroscopy intensity of the plasma sample decreased. This is also an indication that drug-protein binding interaction occurs.

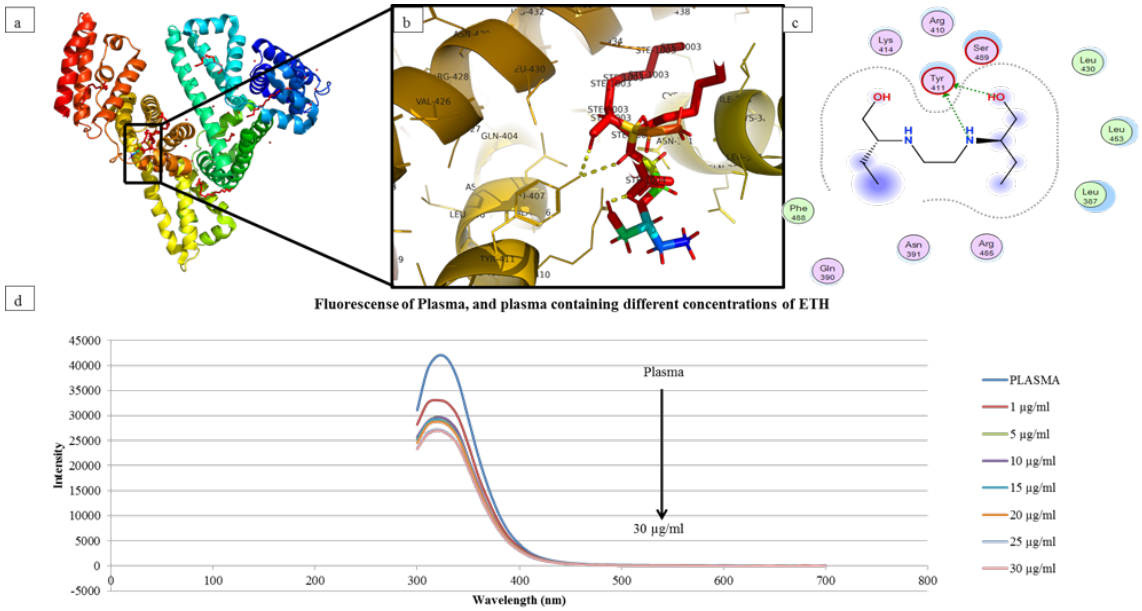

Figure 6: ETH interactions a) Predicted Pymol 3D interaction of ETH with HSA protein binding pocket. b) Amino acid residues and the nature of the interaction between ETH and HSA. c) MOE interaction of ETH with HSA protein pocket c) Experimental fluorescence spectroscopy interaction of ETH in plasma at a concentration range of 1µg/ml-30 µg/ml in increments of 5µg/mL compared to pure plasma standard

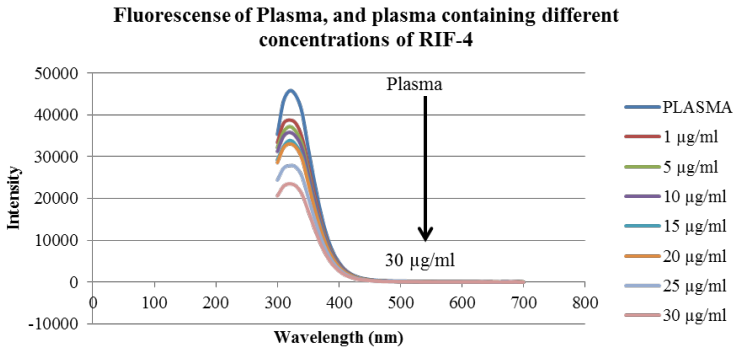

Figure 7: Fluorescence spectroscopy of plasma vs. plasma with different concentrations of RIF-4

Fluorescence Spectroscopy Quenching Constant of Drugs Interacting with the Plasma

Since it is apparent that the entire drug group assessed indicated that quenching occurred, for further analysis, the quenching constant Ksv could then be calculated by using the Stern-Volmer equation 3. Fo indicates the fluorescence spectroscopy intensity before adding the quencher, and F indicates the Fluorescence spectroscopy intensity after the addition of the quencher. [Q] Represents the concentration of the quencher. τo is the fluorophore or plasma's lifetime without the presents of the quencher. Kq indicates the bimolecular quenching constant. To calculate the quenching constant for each drug, a plot of Fo/F vs. [Q] was plotted to obtain the regression of the line.

$$\frac{Fo}{F} = 1 + Kq\,\tau[Q] = 1 + Ksv[Q] \quad \text{...Equation 3}$$

From the obtained fluorescence spectroscopy data the quenching constant Ksv was determined for each drug at the different concentrations of 30-1µg/ml in increments of 5µg/ml between the temperature ranges of 298.15–318.15 K. The following Ksv values as indicated in table 2 were obtained in descending order of the drugs : RIF-4 30.742 x 10^3 M^{-1}, 30.506 x 10^3 M^{-1}, 28.283 x 10^3 M^{-1}, at the temperatures 298.15 K 310.15 K and 313.15 K respectively, RIF 15.083 x 10^3 M^{-1}, 16.140 x 10^3 M^{-1}, 16.801 x 10^3 M^{-1}, at the temperatures 310.15 K 313.15 K and 318.15 K respectively, D-RIF 10.117 x 10^3 M^{-1}, 10.986 x 10^3 M^{-1}, 11.727 x 10^3 M^{-1}, at the temperatures 310.15 K, 313.15 K and 318.15 K respectively, INH 4.6582 x 10^3 M^{-1}, 4.867 x 10^3 M^{-1}, 4.916 x 10^3 M^{-1}, at the temperatures 298.15 K 310.15 K and 318.15 K respectively, PYR 2.8702 x 10^3 M^{-1}, 2.961 x 10^3 M^{-1}, 2.9641 x 10^3 M^{-1}, at the temperatures 298.15 K 313.15 K and 318.15 K respectively and ETH 1.9374 x 10^3 M^{-1}, 1.8896 x 10^3 M^{-1}, 1.9737 x 10^3 M^{-1}, at the temperatures 298.15 K 313.15 K and 318.15 K respectively . From this result, it is evident that RIF-4 has the strongest quenching effect on plasma, followed by RIF, D-RIF, INH, PYR, and ETH had the weakest quenching effect on plasma. All of the drugs indicate dynamic quenching mechanism of fluorescence spectroscopy quenching due to the linearity of the Stern-Volmer plots in Figure 8 (a-f).[37] However Figure 8 (a-f) illustrates the stern

Table 2: Stern-Volmer quenching constant Ksv and linear equations of drugs-plasma at pH 7.4

Drug	*T (K)*	*Linear Equations*	*Ksv X 10^3 (M^{-1})*
INH	298.15	y = 4658.2x + 1.7446 R^2 = 0.9694	4.6582
	310.15	y = 4867x + 1.7031 R^2 = 0.9439	4.867
	318.15	y = 4916.9x + 1.6333 R^2 = 0.9118	4.916
RIF	310.15	y = 15083x + 0.9936 R^2 = 0.9641	15.083
	313.15	y = 16140x + 0.971 R^2 = 0.9517	16.140
	318.15	y = 16801x + 0.972 R^2 = 0.9484	16.801
D-RIF	310.15	y = 10117x + 1.8347 R^2 = 0.8462	10.117
	313.15	y = 10986x + 1.7799 R^2 = 0.842	10.986
	318.15	y = 11727x + 1.7909 R^2 = 0.8378	11.727
PYR	298.15	y = 2870.2x + 1.0514 R^2 = 0.9508	2.8702
	313.15	y = 2961x + 1.0692 R^2 = 0.9727	2.961
	318.15	y = 2964.1x + 1.0784 R^2 = 0.9697	2.9641
ETH	298.15	y = 1937.4x + 1.3329 R^2 = 0.8986	1.9374
	313.15	y = 1889.6x + 1.2084 R^2 = 0.9107	1.8896
	318.15	y = 1973.7x + 1.2925 R^2 = 0.9084	1.9737
RIF-4	298.15	y = 30742x + 1.115 R^2 = 0.8335	30.742
	310.15	y = 30506x + 1.0728 R^2 = 0.8454	30.506
	313.15	y = 28283x + 1.0155 R^2 = 0.8529	28.283

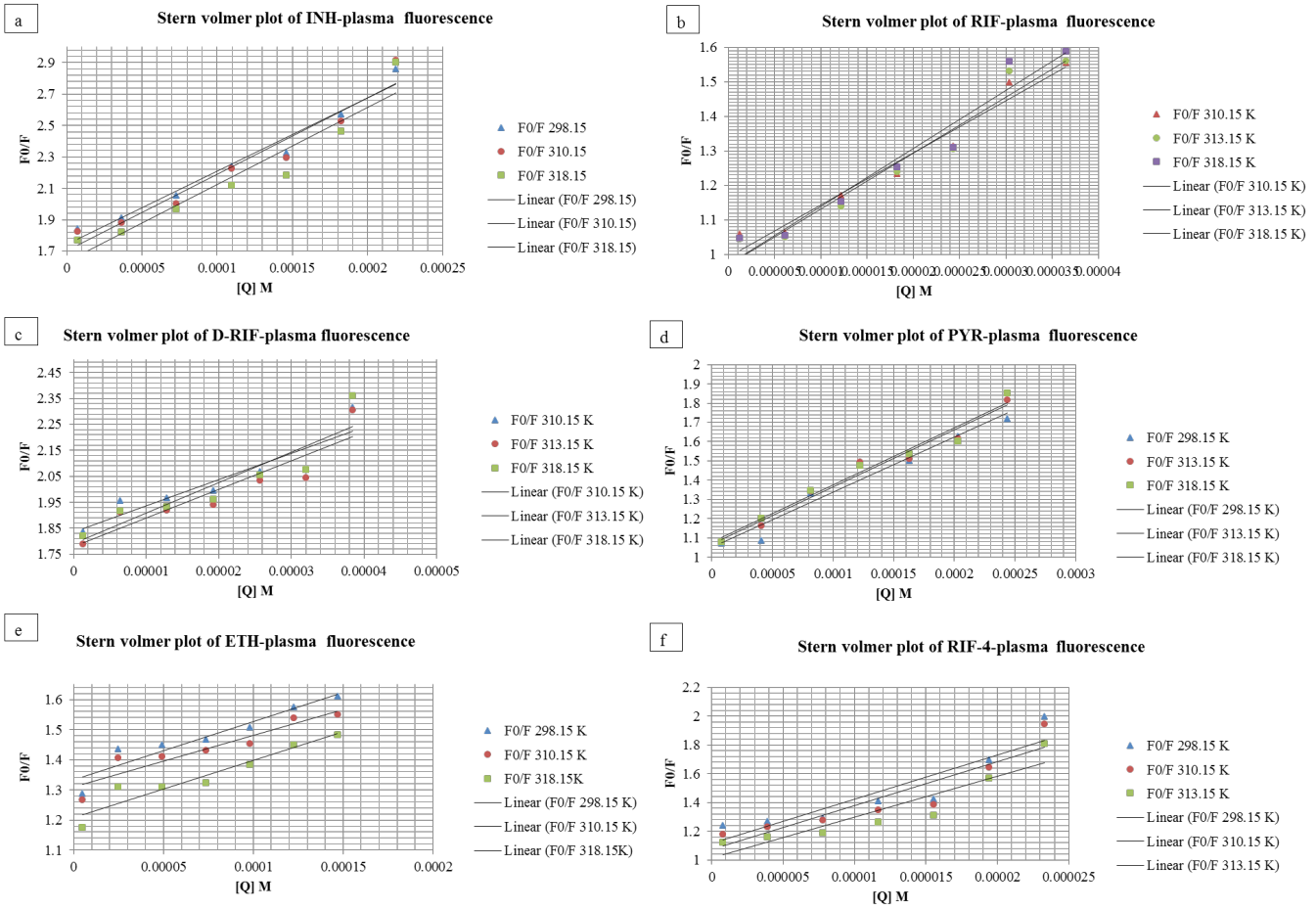

Figure 8: Stern-Volmer plot for quenching of drug with plasma proteins at various temperatures and constant pH 7.4 a) INH concentrations: 1µg/mL (7.292 x 10^{-6} M), 5µg/ml (3.646 x 10^{-6} M), 10µg/mL (7.292 x10^{-5} M), 15µg/ml (10.938 x 10^{-5}), 20 µg/mL (14.584 x10^{-5} M), 25 µg/ml (18.23 x 10^{-5} M) and 30 µg/mL (21.876 x 10^{-5} M) b) RIF concentrations: 1µg/mL (1.215 x 10^{-6} M), 5µg/mL (6.076 x 10^{-6} M), 10µg/mL (1.215 x10^{-5} M), 15µg/mL (1.823 x 10^{-5} M), 20 µg/mL (2.43 x10^{-5} M), 25 µg/mL (3.038 x 10^{-5} M) and 30 µg/mL (3.645 x 10^{-5} M), c) PYR: 1µg/mL (8.123 x 10^{-6} M), 5µg/mL (4.061 x 10^{-6} M), 10µg/mL (8.123 x10^{-5} M), 15µg/mL (12.184 x 10^{-5}), 20 µg/ml (16.245 x10^{-5} M), 25 µg/mL (20.307 x 10^{-5} M) and 30 µg/ml (24.368 x 10^{-5} M), d) D-RIF concentrations: 1µg/ml (1.281 x 10^{-6} M), 5µg/mL (6.403 x 10^{-6} M), 10µg/ml (1.281 x10^{-5} M), 15µg/mL (1.921 x 10^{-5} M), 20 µg/ml (2.561 x10^{-5} M), 25 µg/mL (3.201 x 10^{-5} M) and 30 µg/ml (3.842 x 10^{-5} M), e) ETH concentrations: 1µg/mL (4.895 x 10^{-6} M), 5µg/mL (2.447 x 10^{-5} M), 10µg/mL (4.895 x10^{-5} M), 15µg/mL (7.312 x 10^{-5}), 20 µg/mL (9.789 x10^{-5} M), 25 µg/mL (12.236 x 10^{-5} M) and 30 µg/mL (14.683 x 10^{-5} M), f) RIF-4 concentrations: 1µg/ml (7.767 x 10^{-7} M), 5µg/mL (3.883 x 10^{-6} M), 10µg/mL (7.767 x10^{-6} M), 15µg/mL (1.165 x 10^{-5}), 20 µg/mL (1.553 x10^{-5} M), 25 µg/ml (1.942 x 10^{-5} M) and 30 µg/mL (2.33 x 10^{-5} M

Volmer plot of each drug at 3 different temperatures with the temperature range of 298.15 K-318.15 K. The Ksv of RIF, D-RIF, INH and PYR illustrated that as the temperature increased the Ksv quenching constant increased which is also another confirmation of the dynamic quenching mechanism.[37] ETH in Figure 8 (e) indicated a decrease in Ksv value between 298.15 K and 313.15 K and thereafter an increase in Ksv value between 313.15 K and 318.15 K.

This indicates that ETH could have undergone both dynamic and static quenching.[37] The RIF-4 indicated a decrease in KSV quenching constant as the temperature increased; this is an indication that when all 4 drugs are present, a possibility of static quenching could occur, which could result in a complex formation between RIF-4 and plasma proteins.[37, 38]

$$Lg\left(\frac{Fo-F}{F}\right) = Lg\,K + n\,\lg[Q]$$

...Equation 4

$$\ln K = \frac{-\Delta H^{\circ}}{RT} + \frac{\Delta S^{\circ}}{R}$$

...Equation 5

Determination of the Binding Constant K and the Experimental Thermodynamic Properties of the Drug Interaction with Plasma

To calculate the experimental Gibbs free energy of the drugs, it is required to obtain the bind constant value K as indicated in equation (4) linear regression of the equation was plotted for each drug at three different temperatures ranging between 298.15 K and 318.15 K as indicated in table 3.The following K values were obtained for each drug: RIF 5.379 X 10^2 M^{-1}, 8.422 X 10^2 ,1.585 X 10^3 M^{-1} at temperatures 310.15 K 313.15 K 318.15 K respectively, INH 9.285 M^{-1}, 9.674 M^{-1} ,9.874 M^{-1} at temperatures 298.15 K 310.15 K 318.15 K respectively, 25-Desacety RIF 3.156 M^{-1}, 3.421 M^{-1}, 3.5002 M^{-1} at temperatures 310.15 K 313.15 K 318.15 K respectively,

RIF-4 4.824 X 10^1 M^{-1}, 8.614 X 10^1 M^{-1}, 3.293 X 10^2 M^{-1} at temperatures 310.15 K 313.15 K 318.15 K respectively, ETH 3.443 M^{-1} ,3.516 M^{-1} ,4.857 M^{-1} at temperatures 298.15 K 313.15 K 318.15 K respectively and PYR 3.466 X 10^2 M^{-1}, 3.076 X 10^2 M^{-1}, 1.946 X 10^2 M^{-1} at temperatures 298.15 K 310.15 K 318.15 K respectively. The binding constants calculated at a physiological temperature from the fluorescence spectroscopy data were as follows: Rifampicin 5.379 X 10^2 M^{-1} (moderate affinity), Isoniazid 9.285 M^{-1} (low affinity), 25-Desacetyl Rifampicin 3.156 M^{-1} (low affinity), Ethambutol 3.443 M^{-1} (low affinity) and Pyrazinamide 3.076 X 10^2 M^{-1} (moderate affinity). RIF had the highest binding constant, followed by PYR, INH, ETH, and D-RIF. Therefore when co-administration of the anti-TB drug treatment is used on patients, rifampicin could potentially compete with the other drugs for the binding sites on HSA and plasma protein, which means that hydrophilic drugs like INH, for example, will be unbound and hence not able to reach the site of action and produce its therapeutic effect required by TB patients. This indicates that it could be free to be absorbed into the tissue, and on the other hand, it could be excreted more easily. Once the Binding constant K was obtained for each drug, the thermodynamic parameters could be calculated using the van't Hoff equation 5 were K is the binding constant, and gas and temperature is constant. The ΔH◦ and ΔS◦ values can be calculated from the slope or intercept of the van't Hoff plot of lnK vs 1/T as indicated in Figure 9 (a-f) and the Gibbs free energy equation 5. In Table 4 the change in ΔH◦, ΔS◦ , and Gibbs free energy was experimentally calculated.[34] The ΔH◦ values were positive for all drugs, and the ΔS◦ values were positive for all of the drugs except for the negative ΔH◦ and ΔS◦ of PYR, as indicated in table 4. According to literature, the interaction that PYR undergoes from the fluorescence spectroscopy experimental data was due to van de Waals forces and hydrogen bonding in low dielectric media.[34] It is also an indication that PYR will bind spontaneously at lower temperatures. The drugs that produce positive ΔH◦ and positive ΔS◦ are an indication that the drug will bind spontaneously at higher temperatures

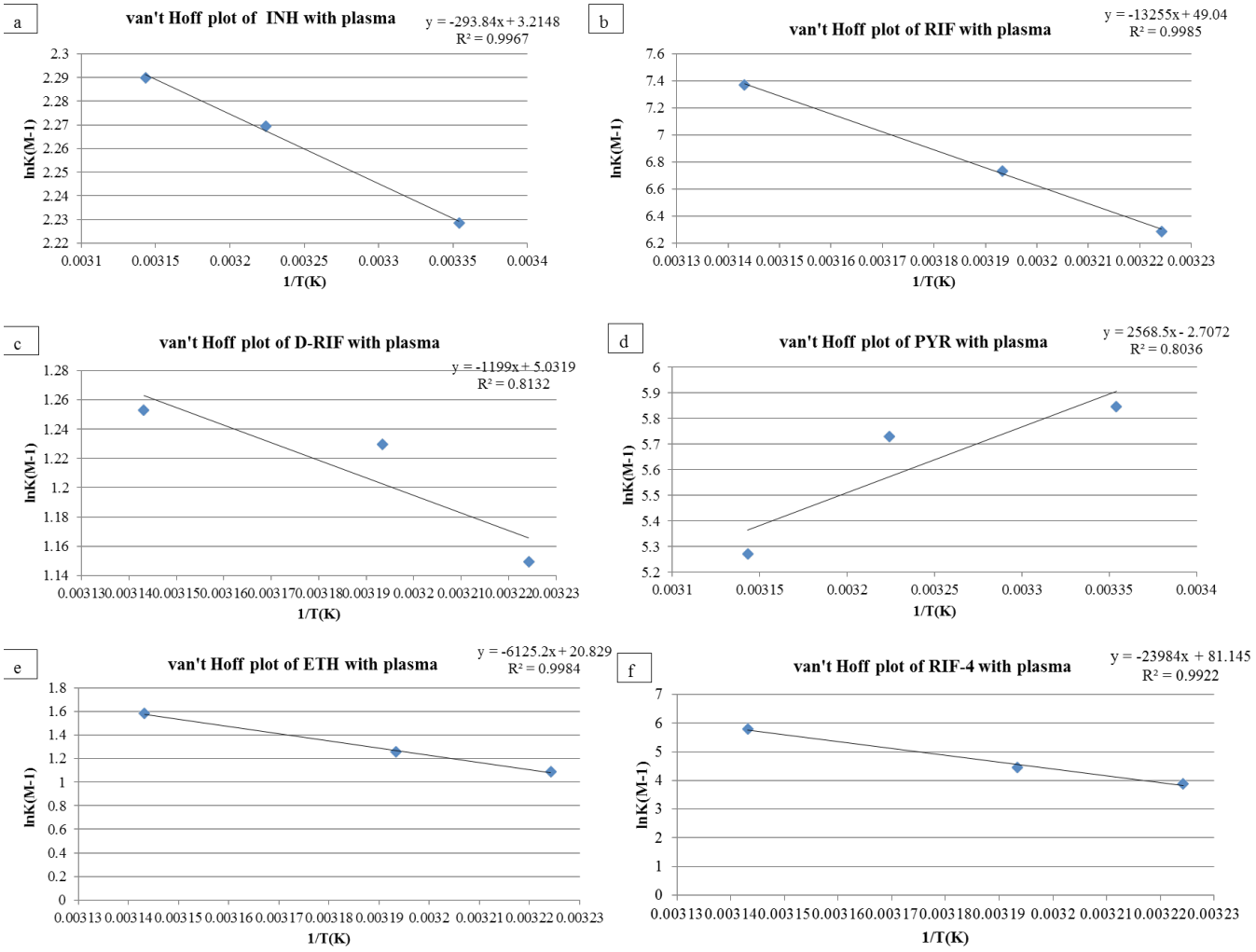

Figure 9: Van't hoff plot lnK vs. 1/T of drug-containing plasma at pH 7.4 a) INH at temperatures of 298.15 K, 313.15 K and 318.15 K b) RIF at temperatures of 310.15 K, 313.15 K and 318.15 K c) D-RIF at temperatures of 310.15 K, 313.15 K, and 318.15 K d) PYR at a temperature of 298.15 K, 310.15 K, and 318.15 K e) ETH at temperatures of 298.15 K, 313.15 K, and 318.15 K f) RIF-4 at temperatures of 310.15 K, 313.15 K, and 318.15 K.

Table 3: Binding parameter K of drugs-plasma at constant temperature

Drug	*T(K)*	*Linear Equations*	*K (M^{-1})*
INH	298.15	y = 0.2138x + 0.9678 R^2 = 0.7891	9.285
	310.15	y = 0.2202x + 0.9856 R^2 = 0.7512	9.674
	318.15	y = 0.2285x + 0.9945 R^2 = 0.7242	9.874
RIF	310.15	y = 0.6983x + 2.7307 R^2 = 0.8402	5.379 X 10^2
	313.15	y = 0.7502x + 2.9254 R^2 = 0.8186	8.422 X 10^2
	318.15	y = 0.7969x + 3.1999 R^2 = 0.8596	1.585 X 10^3
D-RIF	310.15	y = 0.1002x + 0.4991 R^2 = 0.7314	3.156
	313.15	y = 0.1109x + 0.5341 R^2 = 0.7125	3.421
	318.15	y = 0.1108x + 0.5441 R^2 = 0.6718	3.5002
PYR	298.15	y = 0.7495x + 2.5398 R^2 = 0.873	3.466 X 10^2
	310.15	y = 0.731x + 2.488 R^2 = 0.9398	3.076 X 10^2
	318.15	y = 0.6701x + 2.2891 R^2 = 0.9894	1.946 X 10^2
ETH	298.15	y = 0.202x + 0.5369 R^2 = 0.9489	3.443
	313.15	y = 0.2129x + 0.5461 R^2 = 0.9162	3.516
	318.15	y = 0.2703x + 0.6864 R^2 = 0.9283	4.857
RIF-4	310.15	y = 0.4143x + 1.6834 R^2 = 0.7266	4.824 X 10^1
	313.15	y = 0.4864x + 1.9352 R^2 = 0.7301	8.614 X 10^1
	318.15	y = 0.6171x + 2.5176 R^2 = 0.7975	3.293 X 10^2

Table 4: Calculated thermodynamic parameters ΔH◦ (KJ/mol), ΔS◦ (KJ/mol) and Gibbs free energy (KJ/mol) of drugs using the binding constant of drugs-plasma and the van't Hoff equation at specific temperatures

DRUG	*T(K)*	*ΔH◦ (KJ/mol)*	*ΔS◦(KJ/mol)*	*Gibbs free energy (KJ/mol)*
INH	298.15	2.443	0.0267	-5.5244
	310.15			-5.8451
	318.15			-6.0689
RIF	310.15	110.2021	0.0407	-16.2518
	313.15			-17.4749
	318.15			-19.5136
D-RIF	310.15	9.0969	0.0418	-3.0067
	313.15			-3.1322
	318.15			-3.3414
PYR	298.15	-21.3545	-0.0225	-14.6438
	310.15			-14.3738
	318.15			-14.1937
ETH	298.15	50.9249	0.1732	-0.7064
	310.15			-2.7845
	313.15			-3.2780
	318.15			-4.1439
RIF-4	310.15	199.4030	0.6746	-9.8365
	313.15			-11.8604
	318.15			-15.2336

such as body temperature. The positive values for ΔH◦ and ΔS◦ are indicative of a binding process that is controlled by ΔS◦. According to the Gibbs free energy equation, a positive ΔH◦ change is not favorable for the spontaneity of the binding process, unlike a positive ΔS◦ change that leads to a more negative value for the Gibbs free energy.[39] From Ross and Subramanian theory, positive values for ΔH◦ and ΔS◦ change suggest hydrophobic interaction as the main intermolecular force that is involved in the binding process.[39] However, this does not indicate that it is the only type of bonding interaction taking place. The experimental fluorescence spectroscopy data calculated does not correlate with the MOE prediction that the drugs analyzed will infer drug-protein interactions via hydrogen bonding and electrostatic effects. According to literature studies on protein-ligand binding, when the change in ΔS◦ is positive, the reaction is endothermic, which means that the drug will require the heat of the body to interact with the protein, which indicates that disruptions of energetically favorable non-covalent interactions can occur. The Gibbs free energy values obtained for each drug resulted in the following: (RIF-16.2518 kJ/mol -17.4749 kJ/mol -19.5136 kJ/mol at temperatures 310.15 K, 313.15 K, 318.15 K respectively), (INH -5.5244 kJ/mol -5.8451 kJ/mol -6.0689 kJ/mol at temperatures 298.15 K,310.15 K, 318.15 K respectively), (D-RIF -3.0067 kJ/mol -3.1322 kJ/mol, -3.3414 kJ/mol, at temperatures 310.15 K, 313.15 K respectively), (RIF-4 -9.8365 kJ/mol, -11.8604 kJ/mol, -15.2336 kJ/mol, at temperatures 310.15 K, 313.15 K, 318.15 K respectively), (ETH-0.7064 kJ/mol, -2.7845 kJ/mol, -3.2780 kJ/mol -4.1439 kJ/mol at temperatures 298.15 K, 310.15 K, 313.15 K, 318.15 K respectively) and (PYR -14.6438 kJ/mol, -14.3738 kJ/mol, -14.1937 kJ/mol, 298.15 K, 310.15 K, 318.15 K respectively). As a result, the Gibbs free energy for all the drugs is negative, which indicates that the drug plasma binding will occur spontaneously as predicted. It was observed for all drugs that as the temperature increased, the Gibbs free energy increase except for PYR, which decreased in Gibbs free energy. The possibility of competition between drugs for a binding site within the plasma is high due to the low Gibbs free energy values for all drugs. The experimental results indicate that RIF has the lowest Gibbs free energy. ETH has the highest Gibbs free energy, these results deviate with the results predicted however it could be due to the use of plasma which has a higher complexity compared to HSA which is a component of plasma, or incorrect prediction of ΔH◦ or not factoring in the binding constant into the prediction. The use of Fluorescence spectroscopy can also be used to increase the accuracy of the drug-plasma assay by assessing the condition of the plasma to the calibrator plasma used during clinical trials.

UV Analysis of Data

The absorbance spectra were analyzed for all drugs containing plasma with a drug with a concentration of 30 µg/mL-1 µg/ml in increments of 5 µg/ml as well as the drug without plasma and the plasma blank to identify the effect of the absorbance reading of the plasma. The Omega Fluorostar was used to obtain the UV results with a wavelength analysis range of 220-650 nm. As indicated from the absorbance data, a trend was observed for all drugs, whereby as the concentration of the drug increase, the absorbance intensity increased. The absorbance took place between wavelengths of 400-500 nm for the samples and plasma. As indicated in Figure 10, the absorbance spectrum of each drug at the concentration of 30 µg/mL as compared to plasma protein. The sample absorbance of the drugs analyzed had a slight red-shift increase in wavelength at 450nm. The use of the absorbance spectrum is to identify if structural changes in the plasma took place when the drugs were added. This

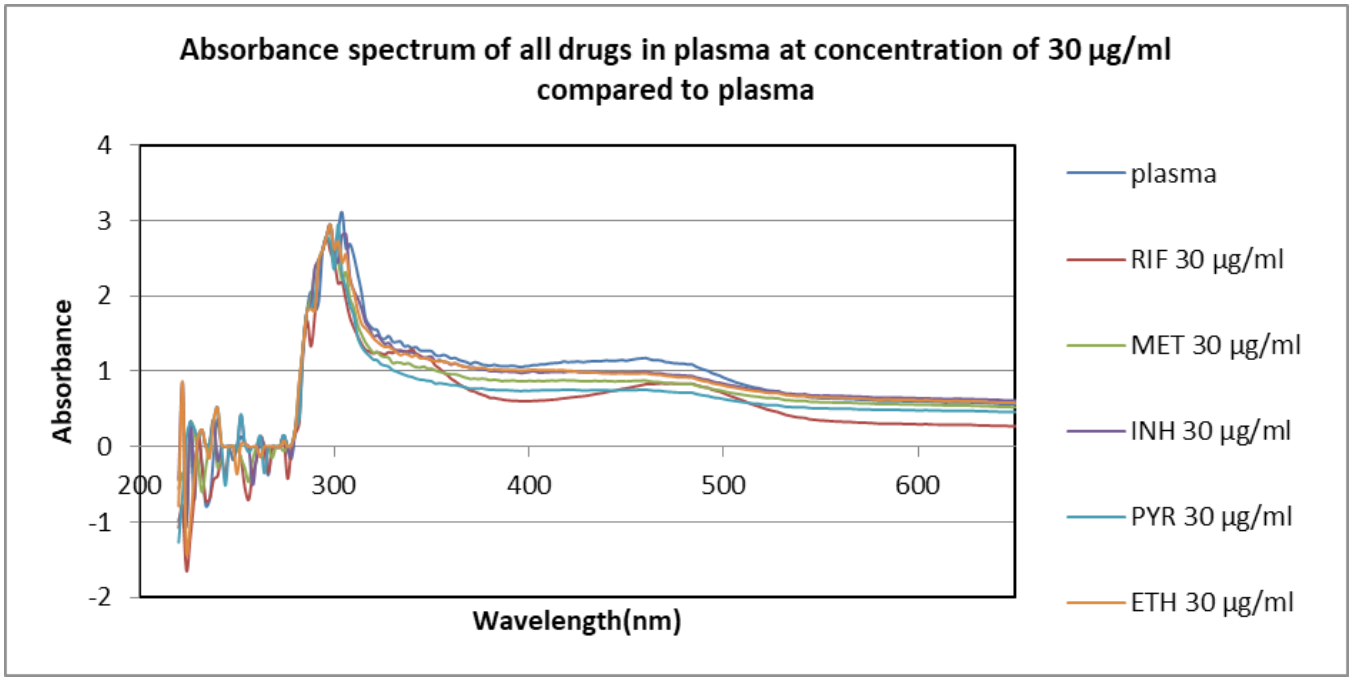

Figure 10: Absorbance spectrum of all drugs (RIF, D-RIF, INH, PYR, and ETH) in plasma at the same concentrations of 30 µg/mL

red-shit indicates that hydrophobicity of the plasma protein decreased.[34]

Significance of using HSA modeling and experimental plasma Fluorescence spectroscopy

The theoretical assessment of HSA molecular docking to the anti-TB drugs showed that HSA does play a significant role in binding to these drugs at specific sites. However, the plasma fluorescence experiment containing HSA and other components such as free fatty acids signifies the need to further investigate the binding of drugs to plasma in addition to HSA. This will further improve the accuracy of the binding energy determination as lower binding energies are possible with other components present in plasma during spontaneous binding interaction. The molecular docking of anti-TB drugs provides an insight into possible binding sites to the HSA pocket as well as its theoretical thermodynamic properties. However, additional information is provided by experimental plasma fluorescence analysis for a realistic approach for the determination of the anti-TB drug binding affinities and thermodynamic properties which links to calibrator use in calibration curves.

CONCLUSION

The predicted computational modeling and fluorescence and UV spectroscopy experimental results both indicated that all of the drugs of interest interact with albumin by hydrogen bonding via electrostatic interactions with specific amino acids present in HSA. Gibbs free energy calculated confirms that the drugs interact spontaneously. The stern-volmer plots indicated that the quenching of plasma is dependent on the concentration and temperature of each drug, which indicates that the more drug available in the body. The higher the possibility of drug-plasma binding, which is unfavorable for TB patients. The KSV quenching constants indicated that RIF, D-RIF, INH, and PYR quenching is enthalpy driven and dynamic quenching occurs. ETH indicates a combination of static and dynamic quenching, which suggests that its binding is entropy-driven. The binding energies experimentally calculated at physiological temperature were as follows: RIF 5.379 X 10^2 M^{-1}, INH 9.285 M^{-1}, D-RIF 3.156 M^{-1}, RIF-4 4.824 X 10^1 M^{-1}, ETH 3.443 M^{-1} and PYR 3.076 X 10^2 M^{-1}. These findings hence confirm that the first-line anti-TB drugs bind to plasma protein present in the body, which causes an overall decrease in the concentration of free drug in the blood. With the assistance of modern software packages, a more accurate determination of the binding constants (equations and pitfalls) can be achieved in the future. Another important finding was that rifampicin had the highest binding affinity to HSA. Therefore when co-administration of the anti-TB drug treatment is used on patients, rifampicin could potentially compete with the other drugs for the binding sites on HSA and plasma protein, which means that hydrophilic drugs like INH, for example, will be unbound and hence not able to reach the site of action and produce its therapeutic effect required by TB patients. The INH prodrug form binding probability is essentially one of the factors that influence the bioavailability of INH and efficacy thereof. The free drug could mean one or two things, it could be free to be absorbed into the tissue, and on the other hand, it could be excreted more easily. We consider that the outcomes of this study provide potential insight into the mechanism responsible for the binding of RIF-4 and D-RIF to albumin and increases the understating of its quantification accuracy in the blood for pharmacokinetic studies. In Addition, Anti-TB drug therapeutic ranges are narrow. Hence our finding on the binding affinity of RIF-4 and D-RIF may provide information to support dosage optimization to achieve efficiency in critically ill patients with extreme protein levels such as hypoalbuminemia. Further validation is needed in the future to accommodate the inner filter effect, collisional quenching, and binding related changes in fluorescence.

ACKNOWLEDGMENTS

We wish to thank the NRF for their financial support. We wish to thank Stellenbosch University staff for their continuous guidance and support.

AUTHOR CONTRIBUTIONS

S. Vallie*, was the principle author,* performed the experiments, project design and wrote the first draft of the manuscript using the data obtained and reported it during his research thesis and dissertation, 2019.S. Naidoo was the principle investigator of this NRF funded project, has contributed to the project design, written and revised the manuscript, and provided all the equipment, reagents, and resources including the fellowship.

REFERENCES

1. Akirov A, Masri-Iraqi H, Atamna A, Shimon I. Low albumin levels are associated with mortality risk in hospitalized patients. The American journal of medicine. 2017 Dec 1;130(12): 1465. e1411-1465.e1419. doi:10.1016/j.amjmed.2017.07.020
2. Velayati AA, Farnia P. Microscopic Anatomy of Mycobacterium tuberculosis. Atlas of Myobacterium Tuberculosis [Internet]. Elsevier; 2017;17–69.
3. Kumar N, Das B, Patra S. Drug Resistance in Tuberculosis: Nanomedicines at Rescue. InAntimicrobial Nanoarchitectonics 2017 Jan 1 (pp. 261-278). Elsevier.
4. Pascual-Pareja JF, Carrillo-Gómez R, Hontañón-Antoñana V, Martínez-Prieto M. Treatment of pulmonary and extrapulmonary tuberculosis. Enfermedades infecciosas y microbiologia clinica (English ed.). 2018 Oct 1;36(8):507-516. doi:10.1016/j.eimc.2017.10.018
5. Caminero JA, Cayla JA, García-García JM, García-Pérez FJ, Palacios JJ, Ruiz-Manzano J. Diagnosis and Treatment of Drug-Resistant Tuberculosis. Archivos de Bronconeumología (English Edition). 2017; 53(9), 501-509. doi:10.1016/j.arbr.2017.07.005
6. Schoenmakers I, Jones KS. Pharmacology and Pharmacokinetics. InVitamin D 2018 Jan 1 (pp. 635-661). Academic Press.
7. Katzung BG. 13 Drugs Used in Heart. Basic & Clinical Pharmacology. 2018:212.
8. Rabbani G, Ahn SN. Structure, enzymatic activities, glycation and therapeutic potential of human serum albumin: A natural cargo. International journal of biological macromolecules. 2019 Feb 15;123:979-990. doi:10.1016/j.ijbiomac.2018.11.053
9. Sugio S, Kashima A, Mochizuki S, Noda M, Kobayashi K. Crystal structure of human serum albumin at 2.5 Å resolution.

Protein engineering. 1999 Jun 1;12(6):439-446. doi:10.1093/protein/12.6.439
10. He XM, Carter DC. Atomic structure and chemistry of human serum albumin. Nature. 1992 Jul;358(6383):209-215. doi:10.1038/358209a0
11. Curry S, Mandelkow H, Brick P, Franks N. Crystal structure of human serum albumin complexed with fatty acid reveals an asymmetric distribution of binding sites. Nature structural biology. 1998 Sep;5(9):827-835.. doi:10.1038/1869
12. Ahmad E, Rabbani G, Zaidi N, Singh S, Rehan M, Khan MM, Rahman SK, Quadri Z, Shadab M, Ashraf MT, Subbarao N. Stereo-selectivity of human serum albumin to enantiomeric and isoelectronic pollutants dissected by spectroscopy, calorimetry and bioinformatics. Plos one. 2011;6(11), e26186. doi:10.1371/journal.pone.0026186
13. Rabbani G, Baig MH, Lee EJ, Cho WK, Ma JY, Choi I. Biophysical study on the interaction between eperisone hydrochloride and human serum albumin using spectroscopic, calorimetric, and molecular docking analyses. Molecular pharmaceutics. 2017 May 1;14(5):1656-1665. doi:10.1021/acs.molpharmaceut.6b01124
14. Rabbani G, Khan MJ, Ahmad A, Maskat MY, Khan RH. Effect of copper oxide nanoparticles on the conformation and activity of β-galactosidase. Colloids and Surfaces B: Biointerfaces. 2014 Nov 1;123:96-105. doi:10.1016/j.colsurfb.2014.08.035
15. Rehman MT, Dey P, Hassan MI, Ahmad F, Batra JK. Functional role of glutamine 28 and arginine 39 in double stranded RNA cleavage by human pancreatic ribonuclease. PloS one. 2011;6(3): e17159. doi:10.1371/journal.pone.0017159
16. Rehman MT, Faheem M, Khan AU. Insignificant β-lactamase activity of human serum albumin: no panic to nonmicrobial-based drug resistance. Letters in applied microbiology. 2013 Oct;57(4):325-329. doi:10.1111/lam.12116
17. Li P, Fan Y, Wang Y, Lu Y, Yin Z. Characterization of plasma protein binding dissociation with online SPE-HPLC. Scientific reports. 2015 Oct 13;5:14866. doi:10.1038/srep14866
18. Lang BE, Cole KD. Unfolding properties of recombinant human serum albumin products are due to bioprocessing steps. Biotechnology progress. 2015 Jan;31(1):62-69. doi:10.1002/btpr.1996
19. Boldt J. Use of albumin: an update. British journal of anaesthesia. 2010 Mar 1;104(3):276-284. doi:10.1093/bja/aep393
20. Alghamdi WA, Al-Shaer MH, Peloquin CA. Protein binding of first-line antituberculosis drugs. Antimicrobial agents and chemotherapy. 2018 Jul 1;62(7):e00641-18. doi:10.1128/aac.00641-18
21. Frieden E. Non-covalent interactions: key to biological flexibility and specificity. Journal of chemical education. 1975 Dec; 52(12): 754. doi:10.1021/ed052p754
22. Akdogan Y, Emrullahoglu M, Tatlidil D, Ucuncu M, Cakan-Akdogan G. EPR studies of intermolecular interactions and competitive binding of drugs in a drug–BSA binding model. Physical Chemistry Chemical Physics. 2016;18(32):22531-22539. doi:10.1039/C6CP04137J
23. Tesseromatis C, Alevizou A. The role of the protein-binding on the mode of drug action as well the interactions with other drugs. European journal of drug metabolism and pharmacokinetics. 2008 Dec 1;33(4):225-230. doi:10.1007/bf03190876
24. Palleria C, Di Paolo A, Giofrè C, Caglioti C, Leuzzi G, Siniscalchi A, De Sarro G, Gallelli L. Pharmacokinetic drug-drug interaction and their implication in clinical management. Journal of research in medical sciences: the official journal of Isfahan University of Medical Sciences. 2013 Jul;18(7):601-610.
25. Sliwoski G, Kothiwale S, Meiler J, Lowe EW. Computational methods in drug discovery. Pharmacological reviews. 2014 Jan 1;66(1):334-395. doi:10.1124/pr.112.007336
26. Marrone TJ, Briggs, and JM, McCammon JA. Structure-based drug design: computational advances. Annual review of pharmacology and toxicology. 1997 Apr;37(1):71-90. doi:10.1146/annurev.pharmtox.37.1.71
27. Soni N, Madhusudhan MS. Computational modeling of protein assemblies. Current opinion in structural biology. 2017 Jun 1;44:179-189. doi:10.1016/j.sbi.2017.04.006
28. Clark, A. M., Labute, P., & Santavy, M. (2006). 2D Structure Depiction. *Journal of Chemical Information and Modeling, 46*(3), 1107-1123. doi:10.1021/ci050550m
29. Nisius B, Sha F, Gohlke H. Structure-based computational analysis of protein binding sites for function and druggability prediction. Journal of biotechnology. 2012 Jun 15;159(3):123-134. doi:10.1016/j.jbiotec.2011.12.005
30. Grünberg R, Nilges M, Leckner J. Flexibility and conformational entropy in protein-protein binding. Structure. 2006 Apr 1;14(4):683-693. doi:10.1016/j.str.2006.01.014
31. Wallace AC, Laskowski RA, Thornton JM. LIGPLOT: a program to generate schematic diagrams of protein-ligand interactions. Protein engineering, design and selection. 1995 Feb 1;8(2):127-134. doi:10.1093/protein/8.2.127
32. Kitchen DB, Decornez H, Furr JR, Bajorath J. Docking and scoring in virtual screening for drug discovery: methods and applications. Nature reviews Drug discovery. 2004 Nov; 3(11): 935-949. doi:10.1038/nrd1549
33. Obermeyer, Z., Samra, J. K., & Mullainathan, S. (2017). Individual differences in normal body temperature: longitudinal big data analysis of patient records. *Bmj, 359*, j5468. doi:10.1136/bmj.j5468
34. Yang GD, Li C, Zeng AG, Zhao Y, Yang R, Bian XL. Fluorescence spectroscopy of osthole binding to human serum albumin. Journal of pharmaceutical analysis. 2013 Jun 1; 3(3): 200-204. doi:https://doi.org/10.1016/j.jpha.2012.10.002
35. Dannenberg JJ, Haskamp L, Masunov A. Are hydrogen bonds covalent or electrostatic? A molecular orbital comparison of molecules in electric fields and H-bonding environments. The Journal of Physical Chemistry A. 1999 Sep 2;103(35):7083-7086. doi:10.1021/jp991010t
36. Rifampin. Tuberculosis. 2008; 88(2): 151-154. doi:https://doi.org/10.1016/S1472-9792(08)70024-6
37. Albani JR. Chapter 4 - Fluorescence Quenching. In J. R. Albani (Ed.), *Structure and Dynamics of Macromolecules: Absorption and Fluorescence Studies*. Amsterdam: Elsevier Science. 2004; pp. 141-192.
38. Behera PK, Mukherjee T, Mishra AK. Simultaneous presence of static and dynamic component in the fluorescence quenching for substituted naphthalene—CCl4 system. Journal of luminescence. 1995 Aug 1;65(3):131-136. doi:https://doi.org/10.1016/0022-2313(95)00067-Z
39. Chaves OA, Tavares MT, Cunha MR, Parise-Filho R, Sant'Anna CM, Netto-Ferreira JC. Multi-spectroscopic and theoretical analysis on the interaction between human serum albumin and a capsaicin derivative—RPF101. Biomolecules. 2018 Sep;8(3):78. doi:10.3390/biom8030078
40. Van de Weert M, Stella L. Fluorescence quenching and ligand binding: A critical discussion of a popular methodology. Journal of Molecular Structure. 2011 Jul 13;998(1-3):144-150. Volume 998, Issues 1–3, https://doi.org/10.1016/j.molstruc.2011.05.023.